Impact of horizontal resolution and model time step on European precipitation extremes in the OpenIFS 43r3 atmosphere model

Yingxue Liu[1,2], Joakim Kjellsson[1,2], Abhishek Savita[1] and Wonsun Park[3,4]

[1]GEOMAR Helmholtz Centre for Ocean Research Kiel, Kiel, Germany

[2]Faculty of Mathematics and Natural Sciences, Christian Albrechts University of Kiel, Kiel, Germany

[3]Center for Climate Physics, Institute for Basic Science (IBS), Busan, Republic of Korea

[4]Department of Integrated Climate System Science, Pusan National University, Busan, Republic of Korea

Correspondence to: Yingxue Liu (yiliu@geomar.de)

Abstract: Events of extreme precipitation pose a hazard to many parts of Europe but are typically not well represented in climate models. Here, we evaluate daily extreme precipitation over Europe during 1982–2019 in observations (GPCC), reanalysis (ERA5) and a set of atmosphere-only simulations at low- (100 km), medium- (50 km) and high- (25 km) horizontal resolution and also at different time steps (i.e., 60, 30 and 15 min) using low resolution (100 km) with identical vertical resolutions using OpenIFS (version 43r3). We find that both OpenIFS simulations and reanalysis underestimate the rates of extreme precipitation compared to observations. The biases are largest for the lowest resolution (100 km) and decrease with increasing horizontal resolution (50 and 25 km) simulations in all seasons. The sensitivity to horizontal resolution is particularly high in mountain regions (such as the Alps, Scandinavia, Iberian Peninsula), likely linked to the sensitivity of vertical velocity to the representation of topography. The sensitivity of precipitation to model resolution increases dramatically with increasing percentiles, with modest biases in the 70th–80th percentile range and large biases above the 99th percentile range. We also find that precipitation above the 99th percentile mostly consists of large-scale precipitation (~80 %) in winter, while in summer it is mostly large-scale precipitation in Northern Europe (~70 %) and convective precipitation in Southern Europe (~70 %). Convective precipitation is more sensitive to model time step than to horizontal resolution. Large-scale precipitation increases significantly with both increasing horizontal resolution and reducing model time step.

1. Introduction

Extreme precipitation events have severe impacts on our society and ecosystems. For example, extreme precipitation caused a devastating flood in Germany in 2021, in which around 180 people died. The frequency and intensity of extreme precipitation are projected to increase over most regions in the future (Intergovernmental Panel on Climate Change, 2023; Li et al., 2021; Myhre et al., 2019). The increasing extreme precipitation poses a threat to society and must thus be realistically simulated and projected accurately for future climates. However, the climate models have large biases in simulating extreme precipitation events due to coarse horizontal resolution grid and long model time step etc. (Alexander et al., 2019; Avila et al., 2015; Sillmann et al., 2013). The model biases are also hard to evaluate as we lack long-term observations. This study aims to understand the sensitivity of extreme precipitation to model horizontal resolution and model time step.

Extreme precipitation events are usually underestimated in CMIP models (O'Gorman, 2015; Sillmann et al., 2013). Some studies found the simulated extreme precipitation at higher atmosphere horizontal resolutions is more realistic (Wehner et al., 2010, 2014). Jong et al. (2023) found that the characteristics of extreme precipitation at 25 km resolution configurations have smaller biases that at 50 and 100 km. While, Kopparla et al. (2013) found that the reduced extreme precipitation biases at higher horizontal resolution do not hold for all regions (e.g., Australia).

Strandberg and Lind (2021) reported the effect of horizontal resolution on European extreme precipitation is largest in regions with complex topography and in the summer season when precipitation is mostly caused by convective processes using coupled models, in agreement with Iles et al. (2020). However, Li et al. (2011) demonstrated that the impact of horizontal resolution on global precipitation extremes is manifested mostly by its effects on large-scale precipitation, which could be due to the improved large-scale circulation (Hack et al., 2006). Other studies also found an increasing large-scale precipitation with higher resolution but the convective precipitation is rather insensitive to resolution (Bacmeister et al., 2014; Jung et al., 2012; Kopparla et al., 2013).

Both the individual physical parameterization in models and their coupling to the dynamics can benefit from a shorter time step (Jung et al., 2012). Mishra and Sahany (2011) found a more realistic simulation of the heavy precipitation in the tropics when the time step was shortened from 60 to 5 minutes at a coarse (~300 km) resolution in a short-period (12 months) configuration. Jung et al. (2012) also reported that the biases in tropical circulation are smaller at 15 minutes than 60 minutes in the IFS model, which is related to tropical precipitation although they did not work on the precipitation in their study. However, Roberts et al. (2018) found a minimal impact on model biases when shorten the time step from 20 to 15 minutes at 25 km in the IFS model. They either did not investigate the multi-year precipitation extremes, or did not explore the extremes in IFS model.

The sensitivity of climate model performance to horizontal resolution and model time step exists in many models, but the level of sensitivity varies considerably between models and studied regions. Most of the global atmosphere-models do not explicitly resolve all the physical processes and must therefore employ parametrizations to represent those unresolved processes (spatially or temporally), which shows a weakness in the models. A recent study by Savita et al. (2024) explored the sensitivity of global mean precipitation to the horizontal resolution and model time step in atmosphere-only simulations with OpenIFS. However, the extreme precipitation's sensitivity to horizontal resolution and time step was not investigated. In this study, we investigated the impact of horizontal resolutions (~100 km, ~50 km, and ~25 km) and model time steps (60 minutes, 30 minutes, and 15 minutes) on daily extreme precipitation using OpenIFS simulations and compare them with observation. We also studied the convective and large-scale precipitation in all simulations. Precipitation extremes sensitivity to model time step is the first time explored in this work using 100 km in OpenIFS atmosphere model. Besides the extremes, we also explored multi-percentile precipitation's sensitivity to horizontal resolution and time step. This paper is structured as follows: section 2 describes the data and methodology, and section 3 discusses the results. The conclusion and discussion can be found in section 4.

2. Data and Methods

2.1 Model, observation, and reanalysis data

The OpenIFS is derived from the Integrated Forecasting System at the European Centre for Medium-range Weather Forecasting (ECMWF-IFS) cycle 43 release 3 (43r3) (ECMWF, 2017). We use the same AMIP simulations that were used in Savita et al. (2024) which cover the period 1979-2014 and are extended to 2019 using sea-surface temperature (SST) from ERA5 and the Shared Socioeconomic Pathway 5 (SSP5-8.5) scenario from CMIP6. OpenIFS simulations use 91 vertical levels (L91) and the different horizontal resolutions: low resolution (Tco95, ~100 km), medium resolution (Tco199, ~50 km), and high resolution (Tco399, ~25 km). For the low resolution, additional sensitivity experiments use different model time steps i.e., 60, 30, and 15 minutes and we refer to these experiments as LR60m, LR30m, and LR, respectively. For medium and high resolution, the same model time step is used (i.e., 15 minutes), of which experiments refer to as MR and HR, respectively. While the OpenIFS uses a reduced octahedral grid (Malardel et al., 2016), the final output used in this study has been interpolated to a regular grid using the second-order conservative method (Kritsikis et al., 2017) by XIOS output server. The LR, LR30m and LR60m output were interpolated to a global 0.9° regular grid while the MR and HR output were interpolated to a global 0.45° regular grid, i.e., we are not investigating extreme precipitation in high resolution simulations in their native reduced octahedral grid, which will be investigated in future study. The simulations used here were used by Savita et al. (2024) who found improvements in the surface zonal wind, Rossby wave amplitude and phase speed, weather regime patterns, and surface-air temperature when reducing a model time step from 60 minutes to 30 and 15 minutes in low resolution or increasing the horizontal resolution from 100 km to 50 and 25 km. However, Savita et al. (2024) did not find such improvement in the mean precipitation bias by increasing horizontal resolution or reducing the model time step.

To validate OpenIFS simulations, we use the gridded daily precipitation observational data from Global Precipitation Climatology Centre (GPCC) with resolution of 1° × 1° for the period 1982–2019 (Ziese et al., 2022) as well as the reanalysis data from the ECMWF Reanalysis v5 (ERA5) for 1979–2019 (Hersbach et al., 2023). ERA5 is based on the IFS Cy41r2, with 31 km horizontal resolution and 137 levels (Hersbach et al., 2020). We analyzed total, large-scale, and convective precipitation in this study. The total precipitation (convective plus large-scale precipitation) in the IFS is the accumulated precipitation, comprising of rain and snow, that falls to the Earth's surface, and it is not assimilated in the IFS. The convective precipitation is generated by the convection scheme in the IFS, which represents convection at spatial scales smaller than the grid box. The convection scheme follows Sundqvist (1978), which is also used in the OpenIFS. The large-scale precipitation is generated by the cloud scheme (Khairoutdinov and Kogan, 2000), which represents the formation and dissipation of clouds and large-scale precipitation due to changes in atmospheric quantities (such as pressure, temperature, and moisture) predicted directly by the IFS at spatial scales of the grid box or larger. The autoconversion/accretion parameterization is a non-linear function of the mass of both liquid cloud and rainwater. The calculation follows Khairoutdinov and Kogan (2000) which is derived from large eddy simulation studies of drizzling stratocumulus clouds, and this scheme is also used in OpenIFS. Several studies have evaluated the performance of ERA5 and found that the total precipitation in ERA5 is performing well over the US (Tarek et al., 2020; Xu et al., 2019). For global precipitation, the mean absolute difference over 50° S–50° N between ERA5 and TRMM/3B43 is 0.58 mm/d; the global-mean correlation with GPCP data is 0.77, which is better compared to ERA-Interim (0.63 mm/d and 0.67) (Hersbach et al., 2020). ERA5 also performs well in polar regions in representing wind, temperature and humidity (Graham et al., 2019; Tetzner et al., 2019; Wang et al., 2019).

Here we analyze daily ERA5 and the OpenIFS data over Europe (30° N–72° N, 10° W–40° E) for the period of 1982–2019 to be consistent with the GPCC dataset. For comparison, the ERA5, GPCC, MR, and HR data are remapped to LR (~0.9375° × 0.9375°) using the second-order conservative remapping method, which is consistent with the XIOS server used. The second-order conservative method includes the gradient across the source cell, which is not included in the first-order conservative method. Therefore, it gives a smoother, more accurate representation of the source field (Jones, 1998).

2.2 Methods

Calculation of q^{th} percentile value

We calculated different percentile values using total precipitation from GPCC, ERA5, and OpenIFS simulations. When we calculated the q^{th} percentile value, the normalized ranking usually did not match the location of the q^{th} percentile exactly, which means the q^{th} lies between two indices. Therefore, we determined the location first, then computed the q^{th} value by interpolating between the two nearest values based on the location. Here we used the formula below to find the location:

$$j = q*(n-1) \tag{1}$$

$\boldsymbol{n}$ is the length of the sample, $\boldsymbol{q}$ is the desired percentile, $\boldsymbol{j}$ is the location which is the distance from the first value X_1 (X_m are the sorted sample values, $\boldsymbol{m}$=1, 2, …, $\boldsymbol{n}$). Then we took $\boldsymbol{i}$ as the nearest (lower) integer of $\boldsymbol{j}$ to get the $\boldsymbol{q}^{\text{th}}$ value P(q) by interpolating.

$$P(q) = X_i + (X_{i+1} - X_i) * (j-i) \tag{2}$$

There are other methods to determine the location of $\boldsymbol{q}^{\text{th}}$ percentile (Hyndman and Fan, 1996), but here we use the 'linear' one.

The large-scale precipitation contribution to extreme precipitation

To calculate the contribution of large-scale precipitation to total precipitation for a percentile range, at each grid point we accumulated the large-scale precipitation on all days when the total precipitation is in that percentile range, then divided it by the accumulated total precipitation on those days to get the fraction of large-scale precipitation.

Calculation of RMSE values

We used the root-mean-square error (RMSE) referenced to GPCC that measures the performance of ERA5 and OpenIFS simulations:

$$\text{RMSE} = \sqrt{\frac{\sum_{i=1}^{n}(x_{mi}-x_{oi})^2}{n}} \tag{3}$$

x_{mi} is the value at *i* grid point for ERA5 or OpenIFS simulations, x_{oi} is the value for GPCC, *n* is the number of land grid points over Europe. Using equation (3), we calculated the RMSE values for different percentile ranges. Smaller RMSE values mean the biases between OpenIFS (or ERA5) and GPCC are smaller i.e., the model simulations and ERA5 are performing better.

Confidence intervals

We calculated the 2.5 to 97.5$^{\text{th}}$ confidence intervals (CI) for the RMSE for each percentile with a bootstrap method. For example, to calculate the CI for the RMSE of HR (referenced to GPCC observation), we randomly chose *n* grid cell pairs from GPCC and HR over European land, then calculated their RMSE (*n* is the number of total land grid points over Europe). This process was repeated for *2000* times. We took the 2.5$^{\text{th}}$ and 97.5$^{\text{th}}$ percentiles of the distribution of the 2000 RMSEs as the 95 % CI. If the CI for different simulations do not overlap then we refer that they are significantly different.

3. Results

3.1 Extreme precipitation over Europe

We show the time series of 99th percentile precipitation calculated from all grid points and all days in each year over the period 1982–2019 from GPCC, ERA5, and OpenIFS simulations over Europe (Fig. 1). The ERA5 simulates an inter-annual variability of the 99th percentile precipitation similar to that in GPCC. For example, the peak in 2010 and the low in 1994 are well reproduced in the ERA5. OpenIFS simulations do not reproduce the same inter-annual variability as in GPCC or ERA5 but LR and HR do reproduce the 95 % significant positive trend observed in GPCC (0.03 mm/d/y, not shown), which are ~0.2 mm/d/y for both LR and HR, and it is not significant for MR. We note that the OpenIFS simulations use observed SST and sea-ice concentrations as boundary conditions, but ozone is taken from a photochemical equilibrium (Cariolle and Teyssèdre, 2007) and aerosol concentrations are taken from Copernicus Atmosphere Monitoring Service (CAMS) monthly climatology. Therefore, we do not expect LR, MR and HR to reproduce trends driven by ozone or aerosols forcing. We also find that both ERA5 and OpenIFS simulations have relatively lower 99th percentile precipitation rates compared to GPCC (Fig. 1). The RMSE for ERA5 (0.36 mm/d) is lower than for OpenIFS simulations which is largest for LR (2.03 mm/d) and decreases with increasing horizontal resolution (i.e., 1.13 mm/d for MR and 0.69 mm/d for HR). Note that Fig. 1 does not contain any spatial information and that a mismatch between model data and observations can be due to the 99th percentile occurring in different regions and/or with different magnitudes. The RMSE analysis suggests that ERA5 and HR are close to GPCC and LR is far from GPCC.

Figure 2a–e shows the spatial distribution of the 99th percentile precipitation over Europe for all days in each season for all years in GPCC, ERA5, and OpenIFS simulations, respectively. In general, the extreme precipitation is very low (~ 2 mm/d) in Northern Africa, which is to be expected since the mean precipitation is only 0.5 mm/d in those regions (Fig. S1). The extreme precipitation exceeds 30 mm/d over mountain areas (e.g., Scandinavian mountains, Alps, and Iberian Peninsula) and the north coast of the Mediterranean but is otherwise lower (~15 mm/d). The spatial distribution of extreme precipitation matches that of the mean precipitation pattern (Fig. S1). The high 99th percentile precipitation near mountains is likely due to the forced ascent of westerly (Scandinavia, Iberian Peninsula, British Isles) and southerly (Alps) winds. The high

99th precipitation in the north of the Mediterranean is likely because of warm and moist southerly winds from the Mediterranean Sea. The ERA5 and OpenIFS simulations overall reproduce the spatial distribution of the 99th percentile precipitation from GPCC. However, the magnitudes are different, particularly over the Scandinavian mountains, the Alps, and central Europe near 50° N (Fig. 2a–e). Figure 2f–i show the regional biases for the 99th percentile precipitation referenced to GPCC. LR mostly underestimates the 99th percentile precipitation in mountainous areas and deserts by more than 25 % (Fig. 2g) and the biases are reduced when horizontal resolution is increased in MR and HR (Fig. 2h–i). We also notice that LR underestimates the 99th percentile precipitation south of the Alps but overestimates it to the north (Fig. 2 (g)), whereas this bias is negligible in higher-resolution simulations (Fig. 2h–i). This could be because the moist southerly winds do not ascend high enough with LR, therefore there is less precipitation formed on the southern side and more moisture is advected over the mountain. The reduced biases near mountain regions in the higher-resolution simulations are likely because higher resolution has a better representation of topography and vertical velocity. A cross section of the topography and annual-mean vertical velocity at 850 hPa and 62° N (Fig. S2 and S3) highlight that the higher-resolution simulations resolve steeper topography, which leads to more ascent and thus more precipitation.

The 99th percentile precipitation over the Alps is more realistic with higher horizontal resolution compared to lower resolution. However, all simulations as well as ERA5 exhibit a negative bias over northeast Italy and west Slovenia (Fig. 2f–i). By analyzing the EOBS data, we find a similar negative bias as in GPCC, but a positive bias in GPCP (Fig. S4d-k). We notice that the extreme precipitation over the Alps (including Slovenia) in GPCP is lower than GPCC and EOBS (Fig. S4a-c), which is likely due to the different data sources and grid methods in different observation datasets (e.g., GPCC and EOBS are gauge-based gridded data on the land, but GPCP data combines microwave and infrared measurements, satellites and rain gauges). We do not know which observation dataset is more realistic, therefore, the cause of the negative bias near Slovenia could be a bias in GPCC or a persistent model bias in the ECMWF-IFS on which both ERA5 and OpenIFS are based. In general, ERA5 has a lower RMSE (2.6 mm/d) for extreme total precipitation than OpenIFS simulations, i.e., ERA5 has overall lower biases than LR (4.0 mm/d) and is similar to MR (3.0 mm/d) and HR (2.9 mm/d).

We next calculate the trend for the annual 99th percentile precipitation over Europe (Fig. 3 & 4) and find that the 99th percentile precipitation has a large positive trend in central Europe and a negative trend to the north of the Alps in GPCC (Fig. 3a). The ERA5 reproduces the pattern of the trend found in GPCC but is not significant. However, OpenIFS simulations do not have consistent patterns with GPCC (Fig. 3c–e, Fig. 4c–e), with only LR30m reproducing the large positive trend in central Europe (Fig. 4c). Overall, the trend is largely underestimated over central Europe but overestimated over northern Europe in OpenIFS simulations. We have not found any consistent improvement across the horizontal resolution and model time step.

In addition to the 99th percentile precipitation and the trend, we calculate annual total precipitation in different percentile ranges, such as 70th–80th, 80th–90th, 90th–95th, 95th–99th, 99th–99.5th, 99.5th–99.9th and larger than 99.9th (i.e., >99.9th) percentile. We calculate the RMSEs for ERA5 and OpenIFS simulations referenced to GPCC in each range and find that the RMSEs for ERA5 and OpenIFS simulations vary strongly across percentile ranges (Fig. 5). The RMSEs increase exponentially with increasing percentiles, from less than 1 mm/d at the 70th–80th percentile range to ~8 mm/d above the 99.9th percentile range. The largest RMSE is found for LR60m above the 99.9th percentile range which is around 12 mm/d [CI: 11.3–12.8 mm/d]. We also find that the RMSEs decrease with finer horizontal resolution for all percentile ranges. The CI of the RMSEs from LR do not overlap with those from higher horizontal resolutions for any percentile range, i.e., the biases from LR are significantly different from that at higher resolutions and thus clearly sensitive to the horizontal resolution. We also find that the RMSE differences between LR simulation and the higher-resolution simulations as well as ERA5 are larger at higher percentile ranges (>95th) than those at lower percentile ranges (<95th). Thus, we conclude that extreme precipitation is more sensitive to horizontal resolution than precipitation at lower percentile ranges (<95th). ERA5 has the smallest RMSE of all datasets above the 95th percentile ranges, i.e., ERA5 has a better representation of the extreme precipitation than our OpenIFS simulations (Fig. 5).

The RMSEs for LR60m, LR30m, and LR are increasing with increasing model time steps. However, the CI of RMSE overlaps at all percentile ranges, i.e., the sensitivity of precipitation to the model time step is not statistically significant in the low-resolution configurations. While the model time step may influence precipitation, especially convective precipitation, errors from poorly resolved topography probably have a large impact on the RMSE, which would explain the lack of sensitivity to the model time step.

3.2 Relative roles of convective and large-scale precipitation

Total precipitation is the sum of convective and large-scale precipitation. Convective precipitation is related to unsolved convective motions. It comes from the physical processes whose scales are smaller than the resolution of the model, therefore need to be parametrized. On the other hand, large-scale precipitation is related to large-scale processes larger than the model resolution, that can be resolved. As the horizontal resolution become higher, large-scale precipitation is likely to increase, and the ratio between convective and large-scale precipitation may change. In this section we split the extreme precipitation into convective and large-scale precipitation to see their sensitivities to horizontal resolution and model time step. The extreme precipitation is nearly 100 % large-scale precipitation over northern Europe, more than 90 % over central Europe, and more than 70 % over western and southern Europe in DJF (Fig. 6e–h). However, in JJA the extreme precipitation is mostly consist of large-scale precipitation over northern Europe (>70 %) and convective precipitation in the Mediterranean region (>70 %) (Fig. 6a–d). Due to the seasonal dependent large-scale precipitation contribution to extreme total precipitation, we discuss convective and large-scale precipitation's sensitivities to horizontal resolution and time step in JJA and DJF separately. The ratios between convective and large-scale precipitation are also discussed here. Considering the ratios over north African region are very large, which influence the results a lot, we remove north Africa and only include the region north than 40°N (i.e., 40° N–72° N, 10° W–40° E) in this section.

During the extreme precipitation days, Europe has more convective precipitation in JJA (~10 mm/d) than in DJF (~3.5 mm/d), and their distributions do not change much across horizontal resolution (Fig. 7a & b). While, from the significant test (Table 2a), we found JJA convective precipitation only increases significantly moving from MR to HR, and DJF convective precipitation significantly increases from LR to MR (HR). However, convective precipitation's distributions vary noticeably across model time steps, as shown in Fig. 7 c & d. As the model time step reduces, the distributions of JJA convective precipitation move to the left, thus less convective precipitation are simulated in shorter time step simulations. DJF has similar results as in JJA. The changes are significant (Table 2a), that is, convective precipitation in OpenIFS is sensitive to model time step.

The distributions of large-scale precipitation in MR and HR (Fig. 7e) shift to the right compared to LR in JJA, and MR and HR have significantly more large-scale precipitation (13.2 mm/d) than LR (11.4 mm/d). In DJF, the distribution peak of LR, MR and HR are similar (Fig. 7f), but MR and HR have bigger tails than LR. Thus, MR and HR have more large-scale precipitation than LR. The increase of large-scale precipitation is likely due to the better simulated topography at higher horizontal resolution, where more large-scale precipitation is resolved. The changes of large-scale precipitation in both JJA and DJF from LR to MR are significant, but not from MR to HR (Table 2b). That means, the large-scale precipitation is sensitive when horizontal resolution is increased from LR to MR, but not from MR to HR. Large-scale precipitation also significantly increases when the model time step is reduced from 60 min to 30 min, and also from 30 min to 15 min in both JJA (Fig. 7g) and DJF (Fig. 7h), that is large-scale precipitation is also sensitive to the model time step.

We further analyse the distribution of ratio between convective and large-scale precipitation in JJA and DJF, shown in Fig. 8. For different resolutions, the ratio distributions from MR and HR are narrower and slightly shift to the left compared to LR in JJA (Fig. 8a), which means MR and HR have smaller mean ratios (1.5) than LR (~1.25). It is likely due to that large-scale precipitation increase by a larger percentage with increasing resolution than convective precipitation. However, the ratio between convective and large-scale precipitation do not vary significantly with changing resolutions in DJF (Fig. 8b). It is likely due to that both large-scale and convective precipitation increase in similar magnitude with increasing horizontal resolution, therefore, the ratio's changes with resolutions are not always significant.

When we reduce the model time step, the distributions of ratios in JJA shift to the left (from 2 to 1.5), which means the ratio decreases with the reducing time step (Fig. 8c). In DJF the peaks of ratio of LR60m, LR30m and LR occur in the similar position (Fig. 8d), but more values fall near the peaks in shorter time step simulations, therefore, ratio decreases when time step is reduced in DJF as well. The ratio decreases significantly as time step reduces in both JJA and DJF (Table 2c), it is related to the significant decreasing convective and increasing large-scale precipitation with reducing model time step.

In summary, during extreme precipitation days, when horizontal resolution increases, convective and large-scale precipitation will increase, while their ratio will decrease. When model time step reduces, convective precipitation will decrease, large-scale precipitation will increase, therefore their ratio will decrease. Convective precipitation is more sensitive to model time steps than to horizontal resolutions, while large-scale precipitation is sensitive to both. Therefore, the extreme precipitation sensitivity to horizontal resolution is mostly from large-scale precipitation.

We also analyse the mean state convective and large-scale precipitation's sensitivity to horizontal resolution and model time step (Fig. S5 & S6). With increasing horizontal resolution and reducing model time step, convective precipitation decreases, large-scale precipitation increases and their ratio decreases. Their sensitivities to resolutions and time steps are less significant in mean state than in extreme state, especially for mean convective precipitation, which is only sensitive when reducing time step from 30 min to 15 min. The changes of mean convective precipitation with horizontal resolution are opposite with the extreme one (Fig. S5a &b, Fig. 7a & b), but these changes for both extreme and mean states are very little, and convective precipitation is more sensitive to model time steps in both states (Fig. S5c & d, Fig. 7c & d).

Additionally, we analyse the precipitation on their native resolution to see the impact of coarsening the horizontal resolution. The native resolution of our model output is 192×384 for LR, 400×800 for MR and HR. Due to the computational expense and time, we only saved a coarser resolution for HR, but not on the original resolution (i.e., ~800×1600). Similar to the result of coarsened data (Fig. 1), extreme precipitation on their native resolution is underestimated in OpenIFS compared to GPCC, and the biases decrease with increasing horizontal resolution (Fig. 9). Extreme precipitation on native resolutions also has similar spatial distribution with that on coarsened resolution (Fig. 10, Fig. 2), such as more extreme precipitation in mountain areas. However, the extreme precipitation is larger (13% for GPCC, 7% for MR and 12% HR) on native resolution than on coarsened resolution, because some extreme precipitation is smoothed during coarsening to 0.9 × 0.9 degree.

Convective and large-scale precipitation during extreme precipitation days increase with increasing horizontal resolution (Fig. 11 a-d) and consistent with coarsened resolution results. The ratio between convective and large-scale precipitation on native resolution significantly decreases from LR to MR in JJA (Fig. 11e), which is also consistent with coarsened resolution.

However, the ratio increases from MR to HR in JJA on native resolution, which is not consistent with coarsened analysis, could be related to the dramatic increasing convective precipitation from MR to HR in JJA. Overall, coarsening the model dataset does not change the conclusion qualitatively in this study, but it does change quantitatively from native to coarsened resolution.

4. Discussion and Conclusion

We have investigated the sensitivity of extreme precipitation across different horizontal resolutions and model time steps in atmosphere-only experiments with the OpenIFS. Comparing extreme precipitation (defined as total daily precipitation at the 99^{th} percentile) from OpenIFS simulations, reanalysis (ERA5), and observation (GPCC), we find that MR and HR mostly better represent the precipitation extremes compared to LR. We also found a more significant sensitivity to the horizontal resolution for the precipitation above the 95^{th} percentile and less sensitivity for lower percentile ranges ($<95^{th}$) (Fig. 5). These OpenIFS-based results are similar to Kopparla et al. (2013), who found that the bias of extreme precipitation in the high-resolution simulation (25 km) is reduced compared to the lower-resolution simulations (100 km and 200 km) over Europe in their atmospheric model, but not for precipitation at lower percentiles (i.e., $<95^{th}$). However, the sensitivity to the horizontal resolution found by Kopparla et al. (2013) was not significant over Europe which is rather different from our results as we have found a significant difference across the horizontal resolutions. In contrast to the extreme precipitation, the bias for global mean precipitation is not decreasing much with increasing horizontal resolution in OpenIFS. Similar results are also found in other AGCMs (e.g., ECHAM6, OpenIFS, HadGEM1 and HadGEM3) (Hertwig et al., 2015; Savita et al., 2024; Schiemann et al., 2014; Demory et al., 2020;). However, Delworth et al. (2012) found an improvement in the global mean precipitation with increasing horizontal resolution in a coupled model (GFDL).

The improvements due to increasing horizontal resolution for the extreme precipitation are mostly over the mountain areas, consistent with previous studies which found the effect of horizontal resolution being largest in areas with complex topography over Europe and also other regions for mean and extreme precipitation (Demory et al., 2020; Iles et al., 2020; Monerie et al., 2020; Prein et al., 2013; Torma et al., 2015). The sensitivity to the horizontal resolution comes from the large-scale precipitation, which is likely because of the better-resolved topography. However, the convective precipitation is more sensitive to the model time step than it is to the horizontal resolution.

In our results, larger improvements are obtained when the horizontal resolution is increased from LR to MR, but relatively smaller improvements from MR to HR. This diminishing return is also found by Roberts et al. (2018) from ~50 km to ~25 km in ECMWF-IFS, but for climatological surface biases. The simulation of extratropical cyclones, tropospheric circulation and tropical mean precipitation in ECMWF-IFS also have smaller improvements from 39 km to 16 km than that from 126 km to 39 km (Jung et al., 2012). However, the tropical cyclone intensity and intense storm structure, which often cause extreme precipitation in tropics (Gori et al., 2022; Zhu and Quiring, 2022) are adequately simulated at 16 km, but not at 126 and 39 km resolutions in ECMWF-IFS (Manganello et al., 2012). Therefore, the diminishing return in this study is valid for European extreme precipitation, but may not for tropical extreme precipitation.

Moreover, the choice of observation dataset is a key factor for assessing the impact of the horizontal resolution and model time step on extreme precipitation. Most observation precipitation data are from one of the three categories, gauge-based products, satellite products, and merged satellite-gauge products. Since the satellite products are constructed with satellite microwave and/ or infrared measurements, with/ without gauged-adjusted estimates, differences exist between these products. Besides, the gauge-based products are highly dependent on the choice of stations and interpolation schemes. It is hard to say which product is closer to reality, as different regions may have different observation datasets that suit best for the analysis. In particular, we note that not all products are suitable for extreme analysis. For example, GPCP's main scope is to construct a reliable climate data record and has been developed with a priority of ensuring the long-term stability of data (Adler et al., 2017). Masunaga et al. (2019) found that the frequency of GPCP daily precipitation quickly drops below all other datasets once the precipitation exceeds 30 mm/d. Also, the time series of GPCP extreme precipitation over the ocean exhibits a jump to lower 99th percentiles in late 2008/early 2009 which is not present in all other datasets, coinciding with the change in utilization of SSM/I and SSMIS. The lower 99th precipitation suggests that the GPCP dataset might not be applied to extreme analysis (Masunaga et al., 2019). Therefore, we only use GPCC observation data as the reference to explore the model performance. In Fig. 2f–i the 99th percentile precipitation is largely underestimated in the eastern Alp region by ERA5 and all model simulations. The biases are insensitive to horizontal resolution. It is likely a persistent model bias in the ECMWF-IFS or a bias in GPCC. Analyzing multiple precipitation products instead of relying on a single one may be a good way to reduce these biases.

Code and data variability

The OpenIFS model requires a software license agreement with ECMWF to use it, and OpenIFS's license is easily given free of charge to any academic or research institute. The details of OpenIFS are available at https://confluence.ecmwf.int/display/OIFS/About+OpenIFS (ECMWF, 2018). We used the same simulation that used in Savita et al. (2024) and therefore do not provide the data needed to reproduce the simulations here. All data (runscripts, input data etc) needed to reproduce the simulations can be found in Savita et al. (2024) in code and data variability section. The jupyter notebook scripts used in this study to produce the plots can be found at https://doi.org/10.5281/zenodo.10887652. The raw model output is available from the authors upon reasonable request. The observation and reanalysis datasets used in this study can be downloaded from GPCC (https://opendata.dwd.de/climate_environment/GPCC/html/fulldata-daily_v2022_doi_download.html, Ziese et al., 2022) and ERA5 (https://cds.climate.copernicus.eu/cdsapp#!/dataset/reanalysis-era5-single-levels?tab=form, Hersbach et al., 2023).

Authors contributions. AS and JK conducted all the OpenIFS simulations. YL did the analysis and writing with substantial contribution from JK, AS and WP.

Competing interests. The contact author has declared that none of the authors has any competing interests.

Acknowledgements. Yingxue Liu is supported by China Scholarship Council (CSC, grant no. 202004910401). Joakim Kjellsson and Abhishek Savita are supported by JPI Climate/Ocean (ROADMAP project, grant no. 01LP2002C). Wonsun Park was supported by IBS (grant no. IBS-R028-D1). We thank the OpenIFS team at ECMWF for the technical support. All the OpenIFS simulations were conducted on the HLRN machine under shk00018 project resources. All the analysis and data storage were conducted on computer clusters at GEOMAR and Kiel University Computing Center (NESH).

Financial support. This research is financially supported by CSC (grant no. 202004910401) and ROADMAP project (grant no. 01LP2002C).

References

Adler, R. F., Gu, G., Sapiano, M., Wang, J. J., and Huffman, G. J.: Global Precipitation: Means, Variations and Trends During the Satellite Era (1979–2014), https://doi.org/10.1007/s10712-017-9416-4, 1 July 2017.

Alexander, L. V., Fowler, H. J., Bador, M., Behrangi, A., Donat, M. G., Dunn, R., Funk, C., Goldie, J., Lewis, E., Rogé, M., Seneviratne, S. I., and Venugopal, V.: On the use of indices to study extreme precipitation on sub-daily and daily timescales, Environmental Research Letters, 14, https://doi.org/10.1088/1748-9326/ab51b6, 2019.

Avila, F. B., Dong, S., Menang, K. P., Rajczak, J., Renom, M., Donat, M. G., and Alexander, L. V.: Systematic investigation of gridding-related scaling effects on annual statistics of daily temperature and precipitation maxima: A case study for south-east Australia, Weather Clim Extrem, 9, 6–16, https://doi.org/10.1016/j.wace.2015.06.003, 2015.

Bacmeister, J. T., Wehner, M. F., Neale, R. B., Gettelman, A., Hannay, C., Lauritzen, P. H., Caron, J. M., and Truesdale, J. E.: Exploratory high-resolution climate simulations using the community atmosphere model (CAM), J Clim, 27, 3073–3099, https://doi.org/10.1175/JCLI-D-13-00387.1, 2014.

Bell, B., Hersbach, H., Simmons, A., Berrisford, P., Dahlgren, P., Horányi, A., Muñoz-Sabater, J., Nicolas, J., Radu, R., Schepers, D., Soci, C., Villaume, S., Bidlot, J. R., Haimberger, L., Woollen, J., Buontempo, C., and Thépaut, J. N.: The ERA5 global reanalysis: Preliminary extension to 1950, Quarterly Journal of the Royal Meteorological Society, 147, 4186–4227, https://doi.org/10.1002/qj.4174, 2021.

Cariolle, D. and Teyssèdre, H.: Atmospheric Chemistry and Physics A revised linear ozone photochemistry parameterization for use in transport and general circulation models: multi-annual simulations, Atmos. Chem. Phys, 2183–2196 pp., 2007.

Delworth, T. L., Rosati, A., Anderson, W., Adcroft, A. J., Balaji, V., Benson, R., Dixon, K., Griffies, S. M., Lee, H. C., Pacanowski, R. C., Vecchi, G. A., Wittenberg, A. T., Zeng, F., and Zhang, R.: Simulated climate and climate change in the GFDL CM2.5 high-resolution coupled climate model, J Clim, 25, 2755–2781, https://doi.org/10.1175/JCLI-D-11-00316.1, 2012.

Demory, M. E., Berthou, S., Fernández, J., Sørland, S. L., Brogli, R., Roberts, M. J., Beyerle, U., Seddon, J., Haarsma, R., Schär, C., Buonomo, E., Christensen, O. B., Ciarlo, J. M., Fealy, R., Nikulin, G., Peano, D., Putrasahan, D., Roberts, C. D., Senan, R., Steger, C., Teichmann, C., and Vautard, R.: European daily precipitation according to EURO-CORDEX regional climate models (RCMs) and high-resolution global climate models (GCMs) from the High-Resolution Model Intercomparison Project (HighResMIP), Geosci Model Dev, 13, 5485–5506, https://doi.org/10.5194/gmd-13-5485-2020, 2020.

ECMWF: IFS Documentation CY43R3 - Part IV: Physical processes, https://doi.org/10.21957/efyk72kl, 2017.

Gori, A., Lin, N., Xi, D., and Emanuel, K.: Tropical cyclone climatology change greatly exacerbates US extreme rainfall–surge hazard, Nat Clim Chang, 12, 171–178, https://doi.org/10.1038/s41558-021-01272-7, 2022.

Graham, R. M., Hudson, S. R., and Maturilli, M.: Improved Performance of ERA5 in Arctic Gateway Relative to Four Global Atmospheric Reanalyses, Geophys Res Lett, 46, 6138–6147, https://doi.org/10.1029/2019GL082781, 2019.

Hack, J. J., Caron, J. M., Danabasoglu, G., Oleson, K. W., Bitz, C., and Truesdale, J. E.: CCSM-CAM3 Climate Simulation Sensitivity to Changes in Horizontal Resolution, 2006.

Hassler, B. and Lauer, A.: Comparison of reanalysis and observational precipitation datasets including era5 and wfde5, Atmosphere (Basel), 12, https://doi.org/10.3390/atmos12111462, 2021.

Hersbach, H., Bell, B., Berrisford, P., Hirahara, S., Horányi, A., Muñoz-Sabater, J., Nicolas, J., Peubey, C., Radu, R., Schepers, D., Simmons, A., Soci, C., Abdalla, S., Abellan, X., Balsamo, G., Bechtold, P., Biavati, G., Bidlot, J., Bonavita, M., De Chiara, G., Dahlgren, P., Dee, D., Diamantakis, M., Dragani, R., Flemming, J., Forbes, R., Fuentes, M., Geer, A., Haimberger, L., Healy, S., Hogan, R. J., Hólm, E., Janisková, M., Keeley, S., Laloyaux, P., Lopez, P., Lupu, C., Radnoti, G., de Rosnay, P., Rozum, I., Vamborg, F., Villaume, S., and Thépaut, J. N.: The ERA5 global reanalysis, Quarterly Journal of the Royal Meteorological Society, 146, 1999–2049, https://doi.org/10.1002/qj.3803, 2020.

Hersbach, H., Bell, B., Berrisford, P., Biavati, G., Horányi, A., Muñoz Sabater, J., Nicolas, J., Peubey, C., Radu, R., Rozum, I., Schepers, D., Simmons, A., Soci, C., Dee, D., Thépaut, J-N.: ERA5 hourly data on single levels from 1940 to present. Copernicus Climate Change Service (C3S) Climate Data Store (CDS), DOI: 10.24381/cds.adbb2d47, 2023 (Accessed on 16-09-2022).

Hertwig, E., von Storch, J. S., Handorf, D., Dethloff, K., Fast, I., and Krismer, T.: Effect of horizontal resolution on ECHAM6-AMIP performance, Clim Dyn, 45, 185–211, https://doi.org/10.1007/s00382-014-2396-x, 2015.

Hyndman, R. J. and Fan, Y.: Sample Quantiles in Statistical Packages, Source: The American Statistician, 361–365 pp., 1996.

Iles, C. E., Vautard, R., Strachan, J., Joussaume, S., Eggen, B. R., and Hewitt, C. D.: The benefits of increasing resolution in global and regional climate simulations for European climate extremes, Geosci Model Dev, 13, 5583–5607, https://doi.org/10.5194/gmd-13-5583-2020, 2020.

Intergovernmental Panel on Climate Change: Weather and Climate Extreme Events in a Changing Climate, in: Climate Change 2021 – The Physical Science Basis, Cambridge University Press, 1513–1766, https://doi.org/10.1017/9781009157896.013, 2023.

Jones, P. W.: First-and Second-Order Conservative Remapping Schemes for Grids in Spherical Coordinates, 1998.

Jong, B. T., Delworth, T. L., Cooke, W. F., Tseng, K. C., and Murakami, H.: Increases in extreme precipitation over the Northeast United States using high-resolution climate model simulations, NPJ Clim Atmos Sci, 6, https://doi.org/10.1038/s41612-023-00347-w, 2023.

Jung, T., Miller, M. J., Palmer, T. N., Towers, P., Wedi, N., Achuthavarier, D., Adams, J. M., Altshuler, E. L., Cash, B. A., Kinter, J. L., Marx, L., Stan, C., and Hodges, K. I.: High-resolution global climate simulations with the ECMWF model in project athena: Experimental design, model climate, and seasonal forecast skill, J Clim, 25, 3155–3172, https://doi.org/10.1175/JCLI-D-11-00265.1, 2012.

Khairoutdinov, M. and Kogan, Y.: A New Cloud Physics Parameterization in a Large-Eddy Simulation Model of Marine Stratocumulus, 2000.

Kopparla, P., Fischer, E. M., Hannay, C., and Knutti, R.: Improved simulation of extreme precipitation in a high-resolution atmosphere model, Geophys Res Lett, 40, 5803–5808, https://doi.org/10.1002/2013GL057866, 2013.

Kritsikis, E., Aechtner, M., Meurdesoif, Y., and Dubos, T.: Conservative interpolation between general spherical meshes, Geosci Model Dev, 10, 425–431, https://doi.org/10.5194/gmd-10-425-2017, 2017.

Lavers, D. A., Simmons, A., Vamborg, F., and Rodwell, M. J.: An evaluation of ERA5 precipitation for climate monitoring, Quarterly Journal of the Royal Meteorological Society, 148, 3152–3165, https://doi.org/10.1002/qj.4351, 2022.

Li, C., Zwiers, F., Zhang, X., Li, G., Sun, Y., and Wehner, M.: Changes in Annual Extremes of Daily Temperature and Precipitation in CMIP6 Models, J Clim, 34, 3441–3460, https://doi.org/10.1175/JCLI-D-19, 2021.

Li, F., Collins, W. D., Wehner, M. F., Williamson, D. L., Olson, J. G., and Algieri, C.: Impact of horizontal resolution on simulation of precipitation extremes in an aqua-planet version of Community Atmospheric Model (CAM3), n.d.

Malardel, S., Wedi, N., Deconinck, W., and Kühnlein, C.: A new grid for the IFS, 2016.

Manganello, J. V., Hodges, K. I., Kinter, J. L., Cash, B. A., Marx, L., Jung, T., Achuthavarier, D., Adams, J. M., Altshuler, E. L., Huang, B., Jin, E. K., Stan, C., Towers, P., and Wedi, N.: Tropical cyclone climatology in a 10-km global atmospheric GCM: Toward weather-resolving climate modeling, J Clim, 25, 3867–3893, https://doi.org/10.1175/JCLI-D-11-00346.1, 2012.

Masunaga, H., Schröder, M., Furuzawa, F. A., Kummerow, C., Rustemeier, E., and Schneider, U.: Inter-product biases in global precipitation extremes, Environmental Research Letters, 14, https://doi.org/10.1088/1748-9326/ab5da9, 2019.

Mishra, S. K. and Sahany, S.: Effects of time step size on the simulation of tropical climate in NCAR-CAM3, Clim Dyn, 37, 689–704, https://doi.org/10.1007/s00382-011-0994-4, 2011.

Monerie, P. A., Chevuturi, A., Cook, P., Klingaman, N. P., and Holloway, C. E.: Role of atmospheric horizontal resolution in simulating tropical and subtropical South American precipitation in HadGEM3-GC31, Geosci Model Dev, 13, 4749–4771, https://doi.org/10.5194/gmd-13-4749-2020, 2020.

Myhre, G., Alterskjær, K., Stjern, C. W., Hodnebrog, Marelle, L., Samset, B. H., Sillmann, J., Schaller, N., Fischer, E., Schulz, M., and Stohl, A.: Frequency of extreme precipitation increases extensively with event rareness under global warming, Sci Rep, 9, https://doi.org/10.1038/s41598-019-52277-4, 2019.

O'Gorman, P. A.: Precipitation Extremes Under Climate Change, https://doi.org/10.1007/s40641-015-0009-3, 1 June 2015.

Prein, A. F., Gobiet, A., Suklitsch, M., Truhetz, H., Awan, N. K., Keuler, K., and Georgievski, G.: Added value of convection permitting seasonal simulations, Clim Dyn, 41, 2655–2677, https://doi.org/10.1007/s00382-013-1744-6, 2013.

Roberts, C. D., Senan, R., Molteni, F., Boussetta, S., Mayer, M., and Keeley, S. P. E.: Climate model configurations of the ecmwf integrated forecasting system (ecmwf-ifs cycle 43r1) for highresmip, Geosci Model Dev, 11, 3681–3712, https://doi.org/10.5194/gmd-11-3681-2018, 2018.

Savita, A., Kjellsson, J., Kedzierski, R. P., Latif, M., Rahm, T., Wahl, S., and Park, W.: Assessment of climate biases in OpenIFS version 43r3 across model horizontal resolutions and time steps, Geosci Model Dev, 17, 1813–1829, https://doi.org/10.5194/gmd-17-1813-2024, 2024.

Schiemann, R., Demory, M. E., Mizielinski, M. S., Roberts, M. J., Shaffrey, L. C., Strachan, J., and Vidale, P. L.: The sensitivity of the tropical circulation and Maritime Continent precipitation to climate model resolution, Clim Dyn, 42, 2455–2468, https://doi.org/10.1007/s00382-013-1997-0, 2014.

Sillmann, J., Kharin, V. V., Zhang, X., Zwiers, F. W., and Bronaugh, D.: Climate extremes indices in the CMIP5 multimodel ensemble: Part 1. Model evaluation in the present climate, Journal of Geophysical Research Atmospheres, 118, 1716–1733, https://doi.org/10.1002/jgrd.50203, 2013.

Strandberg, G. and Lind, P.: The importance of horizontal model resolution on simulated precipitation in Europe – from global to regional models, Weather and Climate Dynamics, 2, 181–204, https://doi.org/10.5194/wcd-2-181-2021, 2021.

Sundqvist, H.: A parameterization scheme for non-convective condensation including prediction of cloud water content, Quarterly Journal of the Royal Meteorological Society, 104, 677–690, https://doi.org/10.1002/qj.49710444110, 1978.

Tarek, M., Brissette, F. P., and Arsenault, R.: Evaluation of the ERA5 reanalysis as a potential reference dataset for hydrological modelling over North America, Hydrol Earth Syst Sci, 24, 2527–2544, https://doi.org/10.5194/hess-24-2527-2020, 2020.

Tetzner, D., Thomas, E., and Allen, C.: A validation of ERA5 reanalysis data in the southern antarctic peninsula—Ellsworth land region, and its implications for ice core studies, Geosciences (Switzerland), 9, https://doi.org/10.3390/geosciences9070289, 2019.

Torma, C., Giorgi, F., and Coppola, E.: Added value of regional climate modeling over areas characterized by complex terrain-precipitation over the Alps, J Geophys Res, 120, 3957–3972, https://doi.org/10.1002/2014JD022781, 2015.

Wang, C., Graham, R. M., Wang, K., Gerland, S., and Granskog, M. A.: Comparison of ERA5 and ERA-Interim near-surface air temperature, snowfall and precipitation over Arctic sea ice: effects on sea ice thermodynamics and evolution, Cryosphere, 13, 1661–1679, https://doi.org/10.5194/tc-13-1661-2019, 2019.

Wehner, M. F., Smith, R. L., Bala, G., and Duffy, P.: The effect of horizontal resolution on simulation of very extreme US precipitation events in a global atmosphere model, Clim Dyn, 34, 241–247, https://doi.org/10.1007/s00382-009-0656-y, 2010.

Wehner, M. F., Reed, K. A., Li, F., Prabhat, Bacmeister, J., Chen, C. T., Paciorek, C., Gleckler, P. J., Sperber, K. R., Collins, W. D., Gettelman, A., and Jablonowski, C.: The effect of horizontal resolution on simulation quality in the Community Atmospheric Model, CAM5.1, J Adv Model Earth Syst, 6, 980–997, https://doi.org/10.1002/2013MS000276, 2014.

Xu, X., Frey, S. K., Boluwade, A., Erler, A. R., Khader, O., Lapen, D. R., and Sudicky, E.: Evaluation of variability among different precipitation products in the Northern Great Plains, J Hydrol Reg Stud, 24, https://doi.org/10.1016/j.ejrh.2019.100608, 2019.

Zhu, L. and Quiring, S. M.: Exposure to precipitation from tropical cyclones has increased over the continental United States from 1948 to 2019, Commun Earth Environ, 3, https://doi.org/10.1038/s43247-022-00639-8, 2022.

Ziese, Markus; Rauthe-Schöch, Armin; Becker, Andreas; Finger, Peter; Rustemeier, Elke; Hänsel, Stephanie; Schneider, Udo: GPCC Full Data Daily Version 2022 at 1.0°: Daily Land-Surface Precipitation from Rain-Gauges built on GTS-based and Historic Data. DOI: 10.5676/DWD_GPCC/FD_D_V2022_100, 2022

Figures

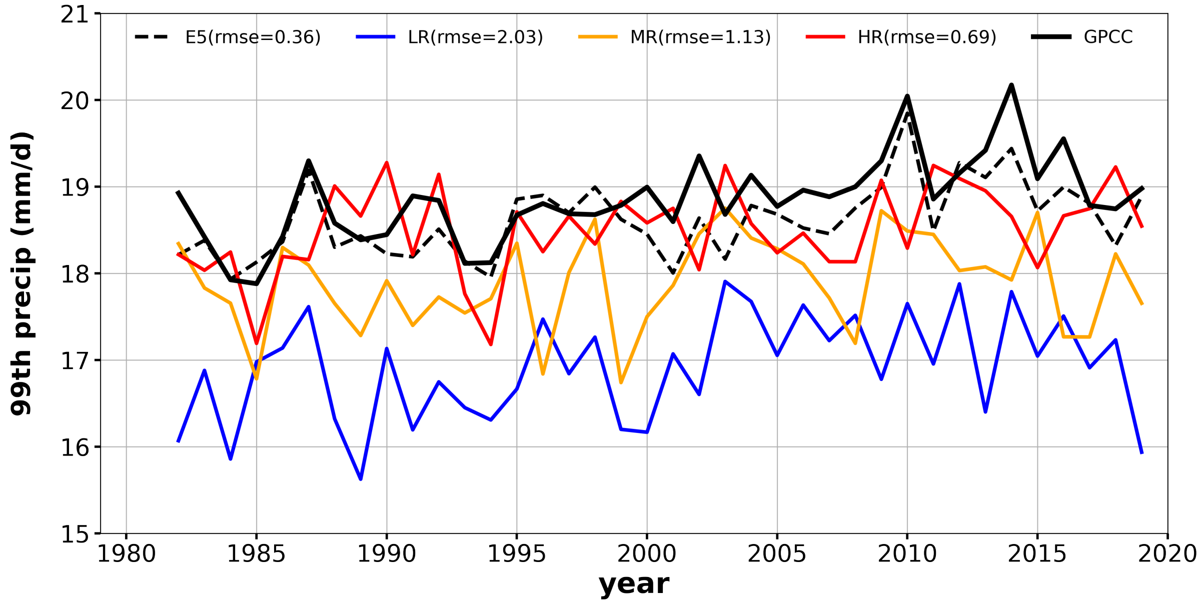

Fig. 1 Annual time series of the 99th percentile precipitation using observations (GPCC, black solid line), reanalysis (ERA5, black dash line), and model simulations (LR: blue, MR: orange, HR: red) during 1982-2019 over Europe. RMSE values of 99th percentile precipitation are computed referenced to GPCC which are shown within the small bracket.

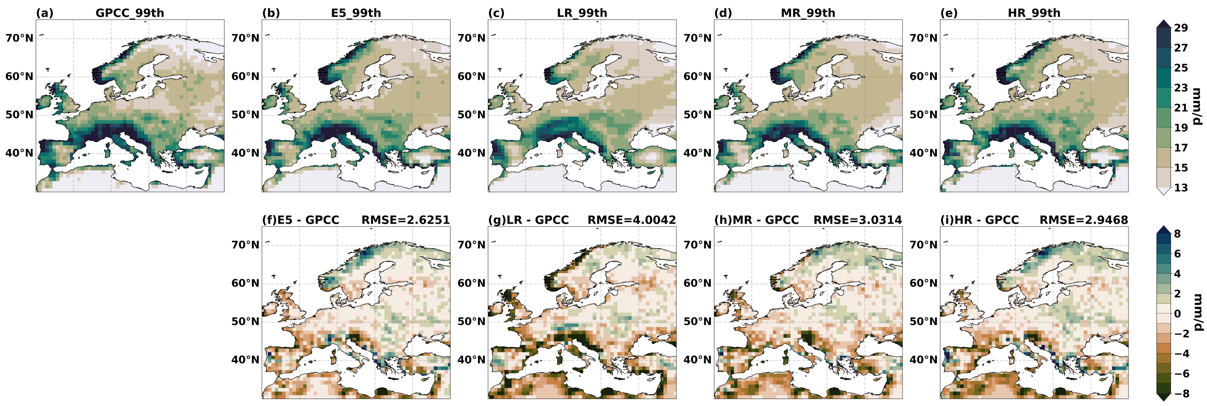

Fig. 2 The 99th percentile precipitation over Europe during 1982-2019 from (a) GPCC observations, (b) ERA5 reanalysis, (c) LR, (d) MR, (e) HR, and the corresponding biases and RMSEs in (f) ERA5, (g) LR, (h) MR, and (i) HR.

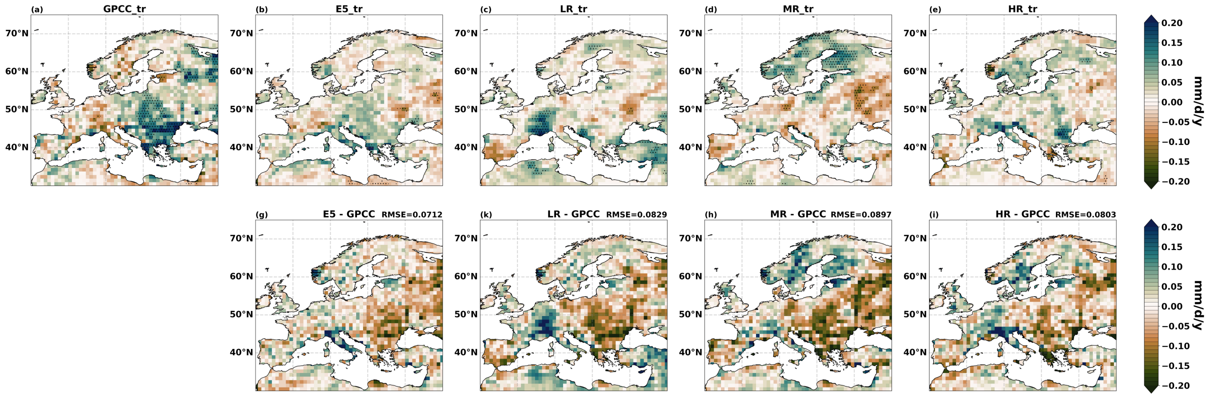

Fig. 3 The linear trends of annual 99th percentile precipitation over Europe during 1982-2019 from (a) GPCC observations, (b) ERA5 reanalysis, (c) LR, (d) MR, (e) HR, and the corresponding biases and RMSEs in (f) ERA5, (g) LR, (h) MR, (i) HR. The shadings are trends at 95 % significance levels.

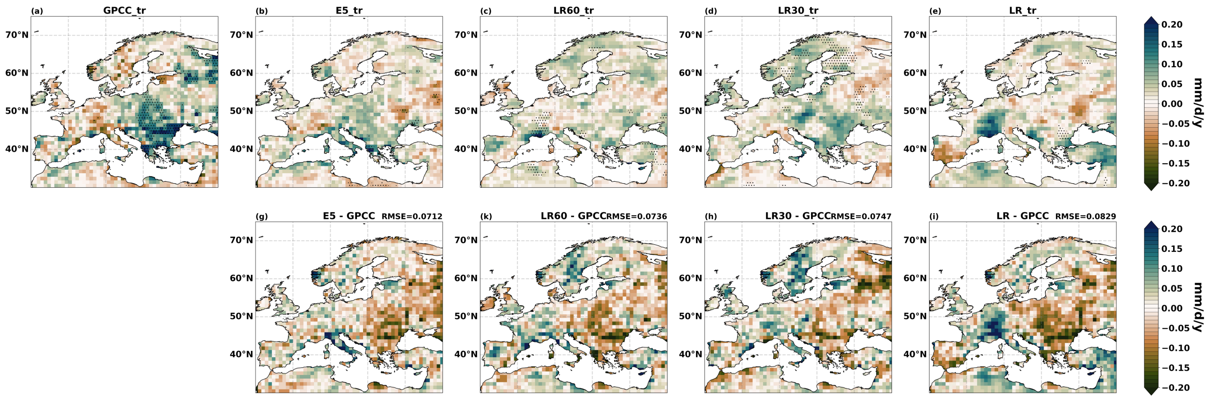

Fig. 4 The linear trends of annual 99th percentile precipitation over Europe during 1982-2019 from (a) GPCC observations, (b) ERA5 reanalysis, (c) LR60m, (d) LR30m, (e) LR, and the corresponding biases and RMSEs in (f) ERA5, (g) LR60m, (h) LR30m, (i) LR. The shadings are trends at 95 % significance levels.

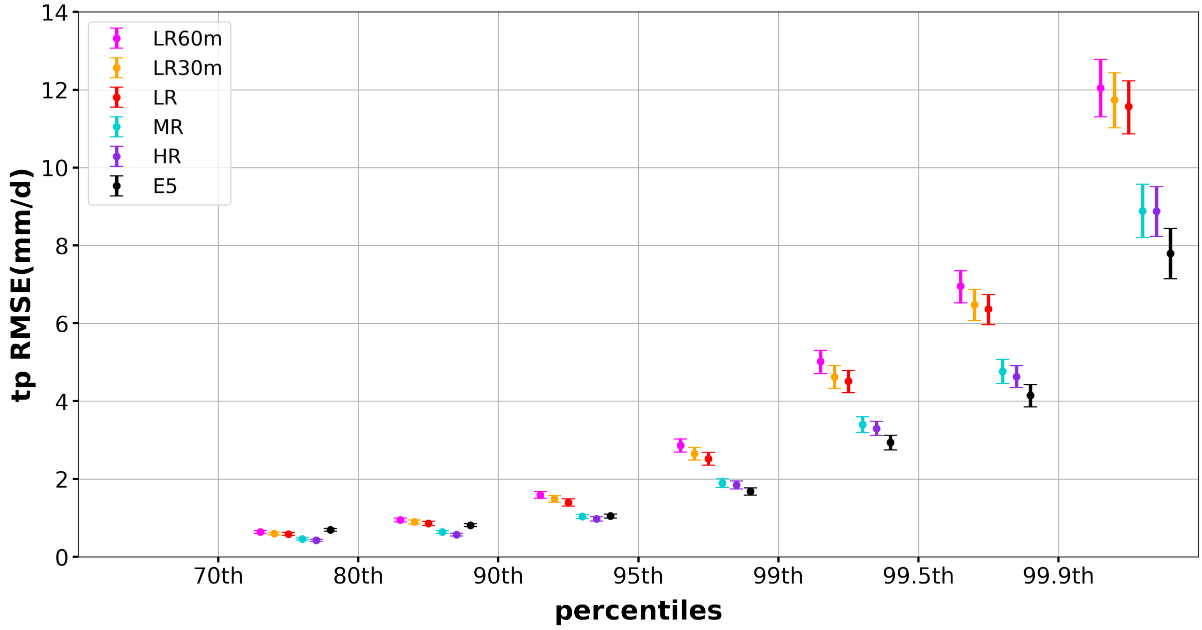

Fig. 5 RMSEs for annual total precipitation at different percentile ranges (70th – 80th, 80th – 90th, 90th – 95th, 95th – 99th, 99th – 99.5th, 99.5th – 99.9th and >99.9th percentile) in ERA5 (black) and OpenIFS simulations (LR60m: magenta, LR30m: orange, LR: red, MR: blue, HR: purple) referenced to GPCC during 1982-2019 over Europe. Dots are the RMSE values, and error bars are the 95 % CI.

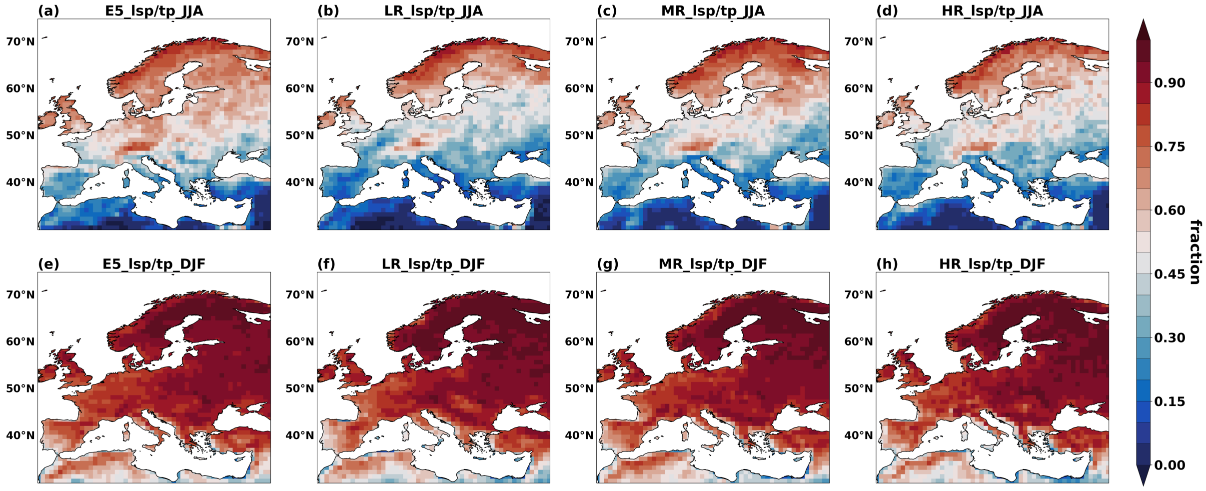

Fig. 6 Contribution of large-scale precipitation to extreme precipitation (>99th percentile) in ERA5 (a & e), LR (b & f), MR (c & g) and HR (d & h) over Europe in JJA (a-d) and DJF (e-h) over the period 1982-2019.

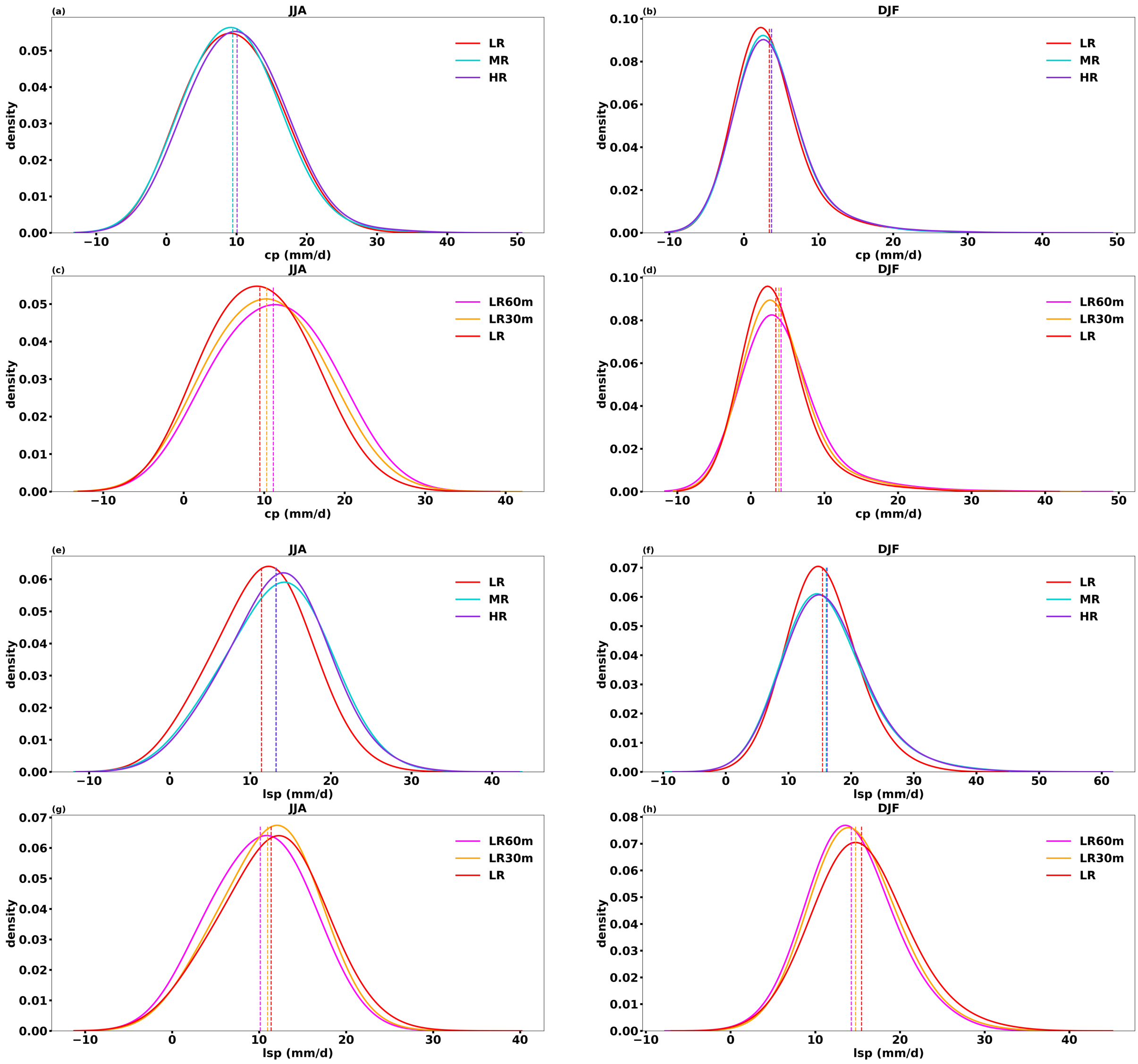

Fig. 7 European convective (a-d) and large-scale precipitation (e-h) distribution across different horizontal resolutions (a, b, e and f) and model time steps (c, d, g and h) during extreme precipitation days in JJA and DJF (LR60m: magenta, LR30m: orange, LR: red, MR: blue, HR: purple). The time period is 1982-2019. The dash lines are the mean values of each distribution.

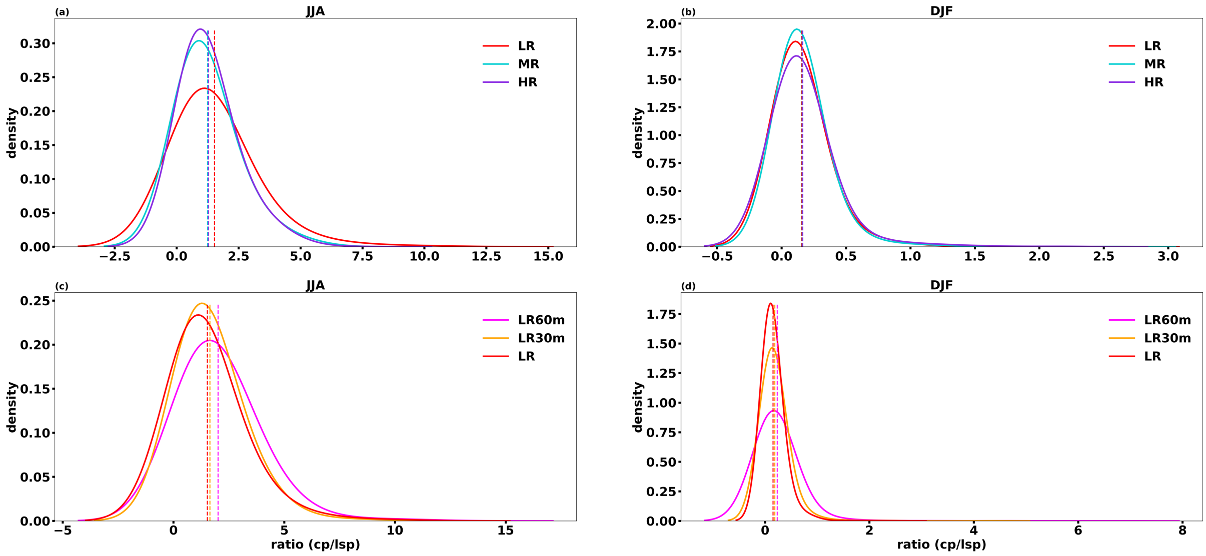

Fig. 8 The ratio between European convective and large-scale precipitation during extreme precipitation days across different horizontal resolutions (a & b) and model time steps (c & d) in JJA and DJF (LR60m: magenta, LR30m: orange, LR: red, MR: blue, HR: purple). The dash lines are the mean values of each distribution.

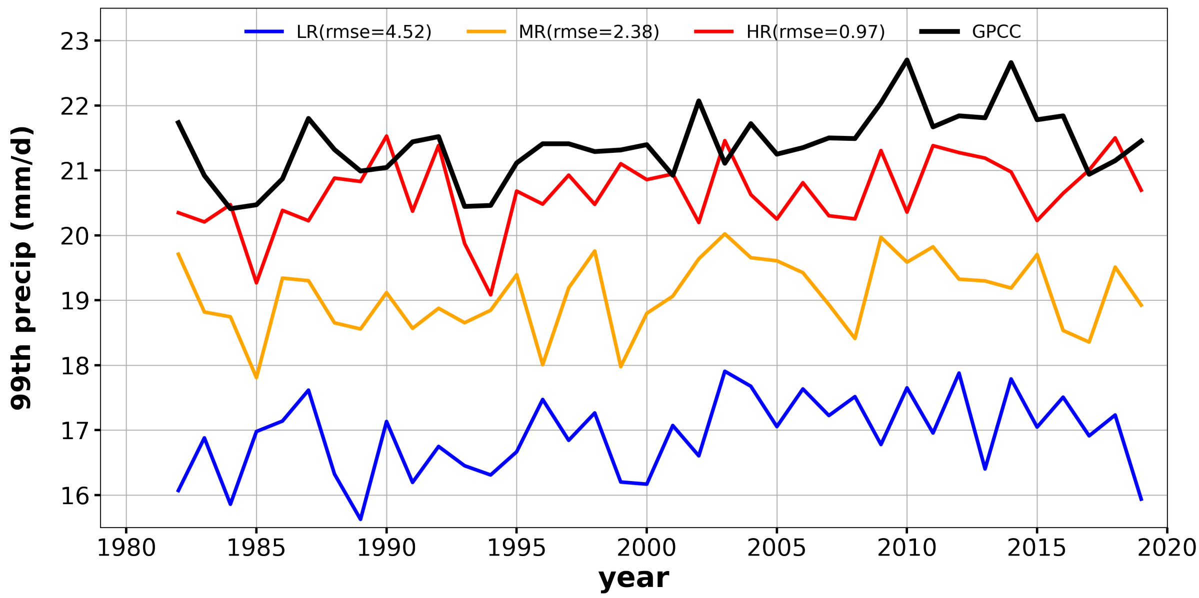

Fig. 9 Annual time series of the 99th percentile precipitation using observations (GPCC, black solid line) and model simulations on their native resolution (LR: blue, MR: orange, HR: red) during 1982-2019 over Europe. RMSE values of 99th percentile precipitation are computed referenced to GPCC which are shown within the small bracket.

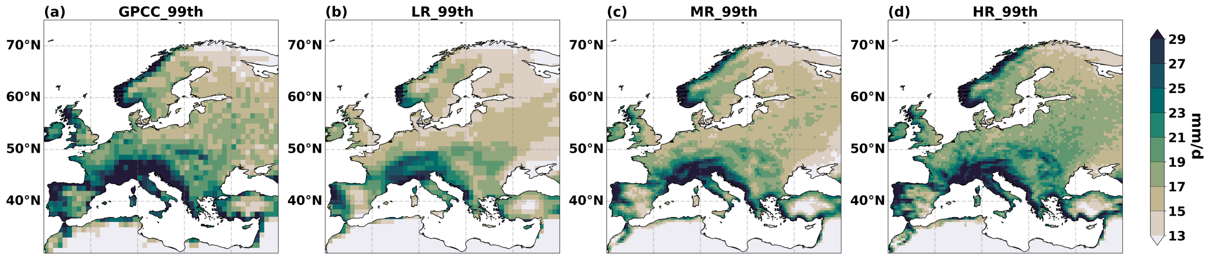

Fig. 10 The 99th percentile precipitation over Europe during 1982-2019 from (a) GPCC observations, (b) LR, (c) MR, (d) HR on their native resolution.

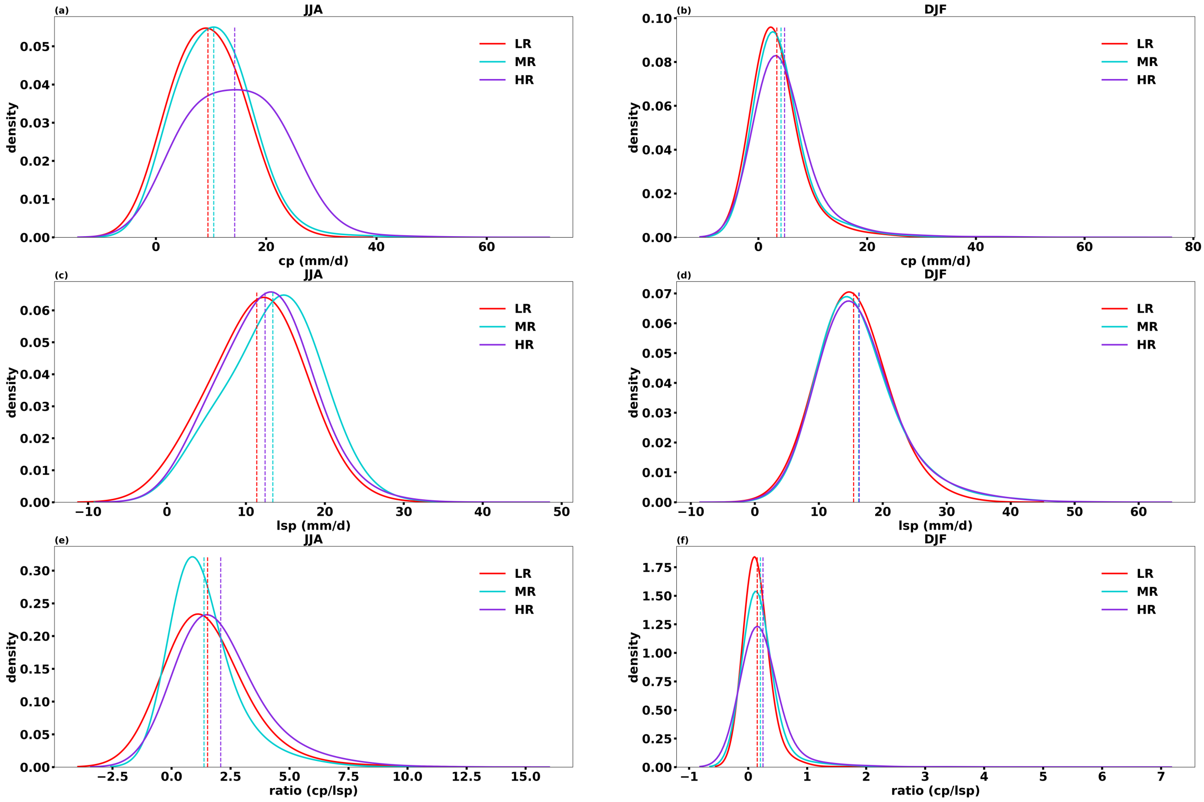

Fig. 11 European convective (a & b), large-scale precipitation (c & d) distribution and ratio (cp/lsp) on their native resolution across different horizontal resolutions during extreme precipitation days in JJA and DJF (LR: red, MR: blue, HR: purple). The time period is 1982-2019. The dash lines are the mean values of each distribution.

Table

Table 1: The experiment details of different horizontal resolutions and model time steps in OpenIFS.

	LR60m	LR30m	LR	MR	HR
Vertical resolution	L91			L91	L91
Horizontal Resolution	100 km (Tco95)			50 km (Tco199)	25 km (Tco399)
Native output resolution	192×384			400×800	400×800
Coarsened resolution	192×384			192×384	192×384
Time steps	60 minutes	30 minutes	15 minutes	15 minutes	15 minutes

Table 2: The p-values of t-test for convective (Table 2a), large-scale precipitation (Table 2b) and their ratios (Table 2c) distribution across horizontal resolutions and model time steps. The bold means significant (p-value < 0.05).

Table 2a

cp	JJA	DJF
LR → MR	0.92	**0.02**
MR → HR	**2.1 e-4**	0.75
LR60m → LR30m	**4.3 e-6**	**0.02**
LR30m → LR	**5.1 e-7**	**0.001**

Table 2b

lsp	JJA	DJF
LR → MR	**1.8 e-29**	**2.2 e-4**
MR → HR	0.70	0.39
LR60m → LR30m	**3.3 e-9**	**9.4 e-5**
LR30m → LR	**0.005**	**3.0 e-7**

Table 2c

ratio	JJA	DJF
LR → MR	**3.0 e-8**	0.49
MR → HR	0.37	0.64
LR60m → LR30m	**1.6 e-10**	**9.0 e-4**
LR30m → LR	**0.03**	**2.0 e-4**